12014 *Biochemistry* **2009,** *48,* 12014–12023
DOI: 10.1021/bi802161u

BIOCHEMISTRY
including biophysical chemistry & molecular biology
Article

Kinetic Analysis of Cysteine Desulfurase CD0387 from *Synechocystis* sp. PCC 6803: Formation of the Persulfide Intermediate†

Elham Behshad*,‡ and J. Martin Bollinger, Jr.

Department of Biochemistry and Molecular Biology, The Pennsylvania State University, University Park, Pennsylvania 16802. ‡Current address: Incyte Corp., Wilmington, DE.

Received November 23, 2008; Revised Manuscript Received October 31, 2009

ABSTRACT: Stopped-flow absorption and isotope effect experiments have been used to dissect the mechanism of formation of the enzyme cysteinyl persulfide intermediate in the reaction of a cysteine desulfurase (CD), CD0387 from *Synechocystis* sp. strain PCC 6803. Seven accumulating intermediates have been identified and tentatively mapped onto the CD chemical mechanism originally proposed by Dean, White, and co-workers [Zheng, L., White, R. H., Cash, V. L., and Dean, D. R. (1994) *Biochemistry 33*, 4714−4720]. The first intermediate with $\lambda_{max} \sim 350$ nm is assigned as either a *gem*-diamine complex or a thiol adduct formed by nucleophilic attack of either the amine group or the sulfhydryl group of the substrate on the internal aldimine form of the pyridoxal 5′-phosphate (PLP) cofactor. The second intermediate, with absorption features at ∼417 and ∼340 nm, is assigned as Cys aldimine and Cys ketimine forms in rapid equilibrium. In agreement with this assignment, a significant substrate α-deuterium equilibrium isotope effect (^{2}H-EIE) favoring the aldimine form (417 nm) is observed in the second state produced in either wild-type CD0387 or the inactive C326A variant protein, which lacks the nucleophilic cysteine residue and is thus unable to proceed beyond this state unless "rescued" by a high concentration of an exogenous thiol. The third intermediate has an additional ∼506 nm feature, characteristic of a quinonoid form, along with the features of the previous state. Its assignment as Ala aldimine, quinonoid, and ketimine forms in rapid equilibrium, which associates its formation with C−S bond cleavage and persulfide formation, is supported by its failure to develop in the C326A variant and the normal *kinetic* isotope effect (^{2}H-KIE) on its formation, which is similar in magnitude to the ^{2}H-EIE disfavoring Cys-ketimine (from which the third state forms) in the second state. Decay of the Ala quinonoid absorption is tentatively attributed to a conformational change by the enzyme that disfavors this form in its equilibrium with Ala aldimine and Ala ketimine. Subsequent decay of the ketimine absorption (∼340 nm) is attributed to release of Ala from the cofactor with an observed rate constant of 10 s^{-1}, the slowest step in the persulfide-forming half-reaction. The enzyme−persulfide·Ala complex dissociates rapidly with a K_d of 98 mM. The final state with λ_{max} ∼350 nm is assigned as a dead-end complex between the enzyme−persulfide and a second L-cysteine, which adds to the cofactor via its sulfhydryl group, possibly forming a cyclic thiazolidine species.

Cysteine desulfurases (CDs)[1] use pyridoxal 5′-phosphate as cofactor to catalyze the conversion of cysteine to alanine and sulfide via a reductively labile enzyme cysteinyl persulfide intermediate. Through the action of additional proteins, the sulfur so mobilized may be incorporated, either directly or indirectly, into iron−sulfur clusters, thiamin, thiouridine, molybdopterin, biotin, and lipoic acid (*2*−*5*). The CD mechanism advanced by Dean and co-workers in their pioneering work on the founding member of the CD family, *Azotobacter vinelandii* NifS (so designated for its role in assembly of the FeS clusters of nitrogenase), invokes 13 intermediates (*1*). The salient features of the mechanism are (1) the formation of a cysteine aldiminium adduct with the cofactor, (2) a net 1,3-prototropic shift from amino acid to cofactor to produce a ketiminium species with the possibility of stabilizing a C-3 centered carbanion by resonance with the iminium moiety, and (3) a previously unprecedented nucleophilic attack by the enzyme cysteine residue on the sulfur of the substrate ketiminium adduct to cleave the C−S bond and form the persulfide (Scheme 1). The mechanism was based heavily on precedent from mechanisms of other pyridoxal phosphate-dependent enzymes, but several key supporting observations were also reported. These included the definitive characterization of the persulfide species by elegant chemical modification experiments and the identification of the nucleophilic cysteine (C325) by mutagenesis of the residue and demonstration that the C325A variant protein has drastically reduced activity. It was further demonstrated that allylglycine and vinylglycine inactivate the enzyme by forming covalent adducts of structures that are consistent with the proton transfer steps proposed to occur in the normal reaction. In addition, it was shown that all unreacted cysteine had undergone exchange of its α proton with solvent deuterium following a long incubation of the enzyme with excess cysteine in ^2H_2O. This observation was interpreted as evidence that the proton transfer steps are fast compared with the C−S bond cleavage step. Finally, it was determined that the enzyme catalyzes exchange

†This research was supported by the National Science Foundation (MCB-0235979 to J.M.B.) E.B. was supported by National Science Foundation Research and Training Grant DBI-902232 (J. G. Ferry, P.I.).

*Address correspondence to this author. Tel: (302) 498-6966. Fax: (302) 425-2721. E-mail: ebehshad@incyte.com.

[1]Abbreviations: CD, cysteine desulfurase; PLP, pyridoxal 5′-phosphate; DTT, dithiothreitol.

 Published on Web 11/02/2009

Scheme 1: Proposed Chemical Mechanism for the Cysteine Desulfurase Reaction[a]

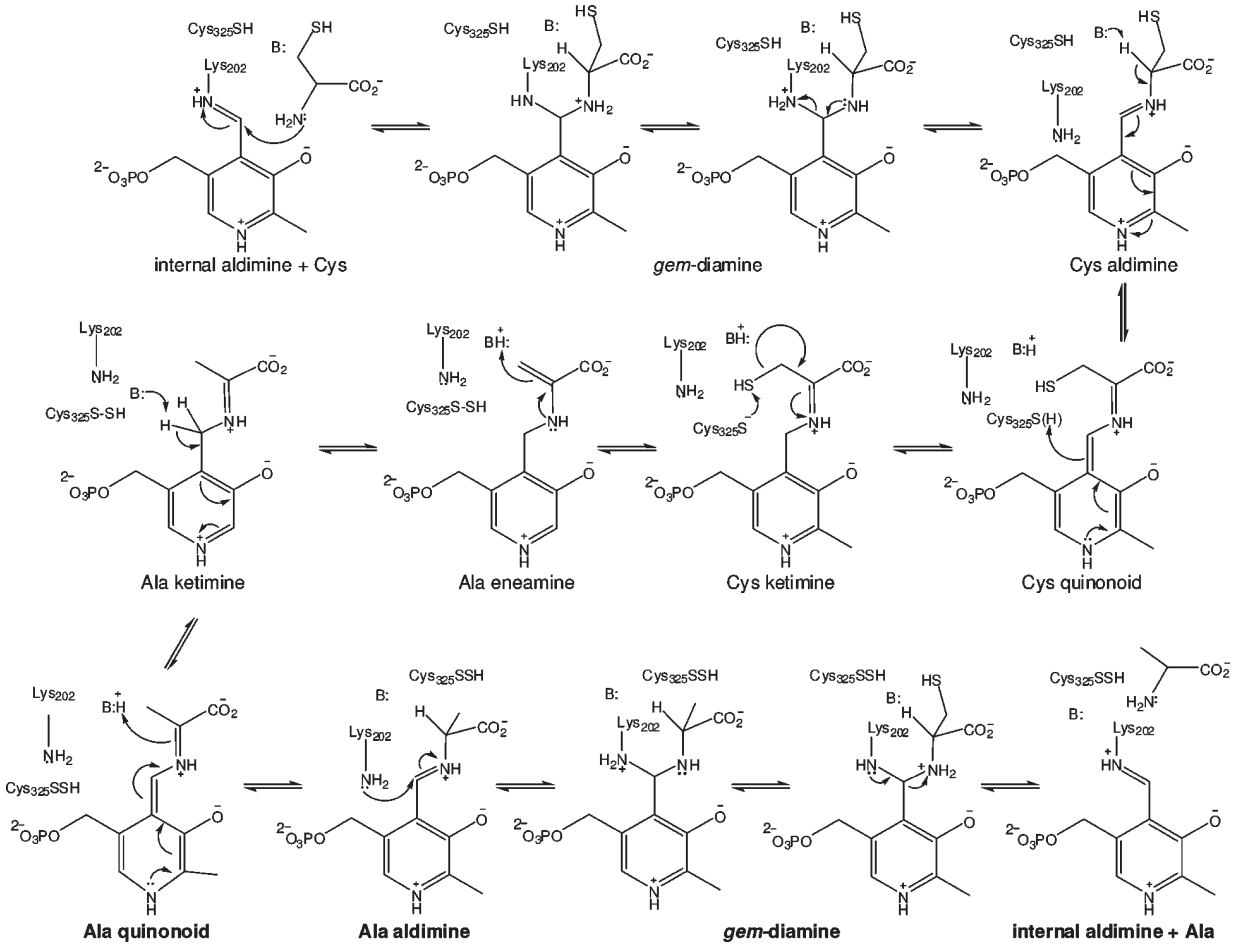

[a]Adapted from Zheng et al. (*1*).

of the α hydron and all three *β* hydrons of alanine without accumulation of partially exchanged intermediates, consistent with the rapid interconversion of Ala aldimine, quinonoid, ketimine, and enamine forms after the slower formation of the Ala aldimine species (*1*).

After the seminal discovery and characterization of *A. vinelandii* NifS (*6*), genes encoding apparent CD homologues were identified in the genomes of nondiazotrophic bacteria, archaea, and eukaryotes including *Saccharomyces cerevisiae* and *Homo sapiens* (*7*, *8*). The vast majority of subsequent studies on CDs focused primarily on the important issues of demonstrating the CD activity of the apparent homologues and tracking the path of the sulfur from the persulfide intermediate to its various destinations (*9*−*12*). New insight into either the CD mechanism or its reaction coordinate (e.g., the nature of the rate-determining step) has been less forthcoming.

In this work, we describe the kinetic dissection of the persulfide-forming half-reaction of one CD, CD0387 from *Synechocystis* sp. strain PCC 6803. This study, along with the characterization of the second half-reaction reported earlier (*13*), permits assessment of the rate-determining step(s) and provides a framework for assessment of the roles of active site residues by similar kinetic dissection of site-directed variants of the CD.

MATERIALS AND METHODS

Materials. [2-^{2}H]-L-Alanine was purchased from Cambridge Isotope Laboratory (Andover, MA). Radiolabeled [^{35}S]-L-cysteine was purchased from New England Nuclear (Boston, MA). The RC58 regenerated cellulose membranes with pore size of 0.2 *μ*m were purchased from Schleicher & Schuell (Keene, NH). L-Cysteine, L-alanine, guanidine hydrochloride, and Sephadex G-25 resin were purchased from Sigma. D_2O was obtained from Isotec Inc. (Miamisburg, OH).

Synthesis of [*2-^{2}H*]-*L-Cysteine*. Cysteine (0.39 g) and 0.145 g of Tris base were dissolved in 85 mL of D_2O. This resulted in a solution with pH of 7.4 which was then divided into two portions. Five micromolar CD0387-C326A variant protein was added to one of the aliquots. After 4−5 h, 0.2% (v/v) trifluoroacetic acid was added to both samples. The samples were then centrifuged to separate the denatured enzyme (present in one sample) from the solution. Both samples were lyophilized. The integrity and purity of [2-^{2}H]-L-cysteine synthesized were examined by NMR: ^{1}H NMR (300 MHz, D_2O) *δ* 2.4 (dd, 2H). Before each experiment, the concentrations of both deuterated and protiated cysteines were determined by use of Ellman's reagent (*14*).

Preparation of the Vector to Overexpress the C326A Variant of CD0387. The codon encoding Cys326 was changed to encode Ala by using the polymerase chain reaction (PCR). pET22b containing the *CD0387* gene was used as the template (*15*). The primers 5′-GGGAAGCTTCAGTGCGGTAGGAAGA**GGC**GGCGGAACC-3′ (*Hin*dIII site underlined, mutation in bold) and 5′-CGGAGCTCGAATTCAACTCCTGGTTAGAAGCA-3′ (*Nde*I site underlined) amplified a 1002 base pair DNA fragment containing the desired substitution (in bold)

and *Nde*I and *Hin*dIII sites for ligation with the vector. The PCR product and pUC18 vector that had both been digested by these two enzymes were joined in a ligation reaction. Competent *Escherichia coli* DH5α cells (PGC Scientific) were transformed with this ligation solution, and plasmid DNA was isolated from the transformants with a Wizard Plus plasmid purification kit (Promega). After the sequence of the PCR product had been verified, the coding fragment was excised from pUC18 by *Nde*I/*Hin*dIII digestion and then ligated with pET22b that had been digested with the same enzymes. The ligation mixture was used to transform competent *E. coli* DH5α cells. The sequence of the coding region was verified to ensure the presence only of the desired substitution. The pET22b-CD0387-C326A plasmid was used to transform the BL21(DE3) (Novagen) expression strain.

Purification of the Wild-Type and C326A Variant Proteins. Wild-type CD0387 and CD0387-C326A were overexpressed and purified as reported previously (*13*).

Spectrophotometry and Stopped-Flow Absorption Measurements. All standard absorption spectra were acquired on a Hewlett-Packard HP8453 spectrophotometer. All stopped-flow experiments were carried out with an Applied Photophysics (Leatherhead, U.K.) SX18MV stopped-flow spectrophotometer housed in the MBraun anaerobic chamber. Reaction conditions are given in the appropriate figure legend.

RESULTS

Spectral Changes Associated with the Reaction of CD0387-C326A with L-Cysteine. To focus on the intermediates formed prior to the C−S bond cleavage step, we employed the C326A variant of CD0387. CD0387-C326A is incapable of nucleophilic attack on the sulfur of the substrate cysteine, and we anticipated that its reaction with cysteine would stall at the step in which the nucleophilic attack would occur in the wild-type protein. We verified that the variant protein produces neither pyruvate, which could result if the protein catalyzes an elimination of sulfide from the substrate, nor 3-mercaptopyruvate, which could result from an abortive transamination reaction. The implication is that the active site of the enzyme prevents these alternative outcomes even when the normal pathway is disabled.

Upon addition of cysteine to CD0387-C326A, a complex with absorption maxima at ~340 and ~417 nm is formed (Figure 1). This complex is stable for several minutes. Titrations of the enzyme with cysteine monitored at either 340 or 417 nm indicate that the complex has a $K_{d,app}$ of 0.32 ± 0.05 mM (inset in Figure 1). The positions of its absorption features suggest that the complex is a mixture of at least two species, of which at least one has extended conjugation with the pyridoxal ring and at least one does not. This inference, the expectation that the intermediate(s) immediately preceding C−S bond cleavage should accumulate in the C326A variant, and the mechanistic proposal by Dean and White together lead to the conclusion that this complex is a mixture of Cys aldimine and Cys ketimine species in equilibrium.

This assignment is supported by spectra obtained upon reaction of CD0387-C326A with [2-^{2}H]-L-cysteine in H_2O and CD0387-C326A with L-cysteine in D_2O. The same absorption features are observed, but the ratio of intensities is significantly different, and the higher energy feature appears to be slightly red shifted (Figure 2A). The change in relative intensities indicates that the α-C−H bond is cleaved during formation of this state and that there is a deuterium equilibrium isotope effect (^{2}H-EIE) on the ratio of the individual species that the state comprises. The

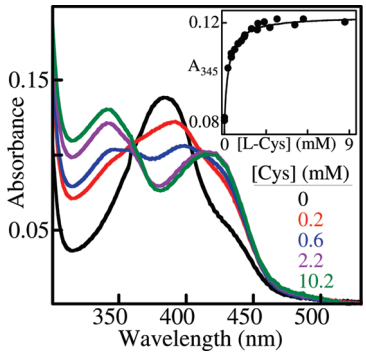

FIGURE 1: Changes in the absorption spectrum of CD0387-C326A associated with formation of reaction with the substrate, cysteine. Increasing concentrations of cysteine were added to 50 μM C326A in 100 mM HEPES, pH 7.8 at room temperature, and spectra acquired in less than 30 s. The inset shows a plot of absorbance at 345 nm as a function of cysteine concentration. The solid line is a fit of the equation for a hyperbola to the data.

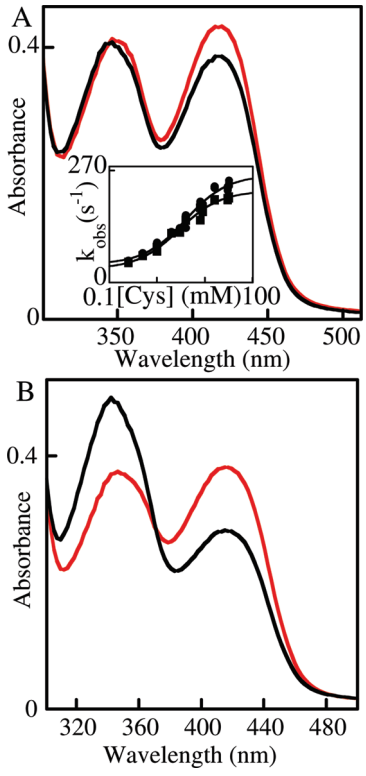

FIGURE 2: (A) Reaction of C326A variant with [2-^{2}H]cysteine reveals the existence of a primary equilibrium isotope effect of 1.7−2 on the Cys aldimine/Cys ketimine ratio in the second intermediate state. Thirty millimolar [2-^{2}H]cysteine (red trace) or [2-^{1}H]cysteine (black trace) was added to 100 μM C326A in 100 mM HEPES, pH 7.8 at 21 °C. The inset shows the concentration dependence of the first-order growth rate constants ([2-^{2}H]cysteine in circles and [2-^{1}H]cysteine in squares). (B) Solvent equilibrium isotope effect on Cys aldimine/Cys ketimine ratio upon addition of cysteine to CD0387-C3326A in ^2H_2O (black trace) versus H_2O (red trace). Twenty-five millimolar cysteine was added to 100 μM CD0387-C326A in 100 mM HEPES, pH 7.8 (or pD 7.8) at 21 °C.

apparent shift in the higher energy feature is attributable to a slightly greater population of an additional species with λ_{max} = 350 nm that is an intermediate between the resting enzyme and the stable complex (*vide infra*). Relaxation of the spectrum of the complex produced from [2-^{2}H]-L-cysteine to that characteristic of the complex formed with unlabeled L-cysteine, which presumably

results from exchange with solvent, occurs over seconds, even when only a 10-fold excess of substrate over enzyme is used. These observations indicate that the rate constant for exchange of the α-deuteron with solvent protons is small relative to those for formation and breakdown of the complex. The converse exchange reaction has been demonstrated in our preparation of the specifically deuterated cysteine by incubation of unlabeled substrate with CD0387-C326A in ^2H_2O. In this reaction, the initial complex formed (prior to slow exchange of the α-protium with solvent deuterium) has an opposite perturbation compared to that observed in the reaction of CD0387-C326A with the deuterated substrate in ^1H_2O (Figure 2B). The 340 nm band characteristic of the Cys ketimine species is markedly more intense and the 417 nm band characteristic of aldimine much less intense in ^2H_2O, suggesting a significant deuterium equilibrium isotope effect on this step. Again, in this reaction the spectrum relaxes over many seconds as exchange proceeds slowly relative to formation of the initial complex. As elaborated in the Discussion section, these observations have implications with respect to the identity of the active site residues that mediate the net 1,3-prototropic shift in preparation for C−S bond cleavage.

Chemical Rescue of Cysteine Desulfuration in CD0387-C326A. We reasoned that, if the C326A variant can proceed through the normal desulfurase reaction sequence only to the point at which the nucleophilic attack by C326 would normally occur, then it might be possible to demonstrate "chemical rescue" of desulfurase activity by inclusion of high concentrations of exogenous nucleophilic thiols. Upon addition of 0.3 and 3 mM ^{35}S-radiolabeled cysteine to 0.15 mM C326A and incubation with 50 mM BME for 10 min, 0.053 and 0.11 mM H_2S were produced, respectively. Under the same reaction conditions but with 50 mM DTT in place of BME, 0.029 and 0.072 mM H_2S were produced, respectively. Upon addition of 0.3 and 3 mM ^{35}S-radiolabeled cysteine to 1 μM CD0387 and incubation with 50 mM BME for 10 min, 18 and 22 μM H_2S were produced, respectively. Under the same reaction conditions but with 50 mM DTT in place of BME, 0.3 and 0.48 mM H_2S were produced, respectively. Production of H_2S was monitored using an assay reported in our earlier work (*13*). The simplest interpretation of these data is that thiol groups from BME or DTT can substitute for the nucleophilic thiol group of Cys326, albeit with much less efficiency. DTT appears to be less efficient than BME. This is most likely due to the fact that DTT has greater affinity for the PLP cofactor (K_d of 13 mM for DTT versus 160 mM for BME; data not shown) and therefore blocks cysteine binding when present at concentrations sufficient to see significant rescue of C−S cleavage. Regardless, the observation of cysteine desulfuration by CD0387-C326A in the presence of either thiol lends support both to the notion that the variant protein is incompetent only for the nucleophilic attack step and, indirectly, to the assignment of its stable complex with cysteine to a mixture of Cys aldimine and Cys ketimine forms.

Kinetics of Reaction of CD0387-C326A with L-Cysteine. Interrogation of the reaction of CD0387-C326A with cysteine by stopped-flow absorption spectrophotometry revealed that a single detectable intermediate state forms on the way to the stable complex (Figure 3). The intermediate forms in the dead time of the stopped-flow apparatus (1.3 ms) and is characterized by an absorption feature that is significantly red shifted ($\lambda_{max} \sim$ 350 nm) relative to the 340 nm feature of the stable complex. The position of this absorption band implies that conjugation between the imine and the pyridoxal ring has been lost. Given that

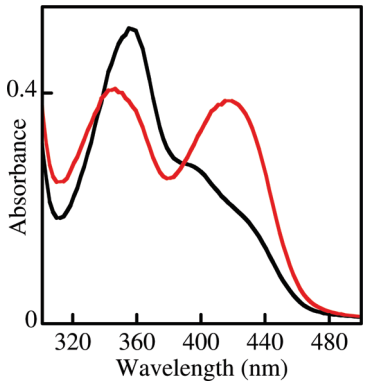

FIGURE 3: Absorption spectra for the two intermediates (thiol adduct and equilibrium mixture of Cys aldimine and Cys ketimine) obtained from the data collected by multiwavelength stopped flow. The spectra were collected at 1.9 ms (black trace) and 80 ms (red trace). Thirty millimolar cysteine was added to 100 μM C326A in 100 mM HEPES, pH 7.8 at 21 °C.

α proton abstraction occurs in the next step, the only likely mechanism for loss of conjugation in this step is addition of cysteine to the internal aldimine. The most obvious candidate structure is of a *gem*-diamine, and precedent suggests that these species can accumulate (*16*). The observed intermediate state accumulates nearly to stoichiometric levels (as evidenced by the nearly complete loss of the ~385 nm peak of the resting enzyme). Alternatively, the 350 nm absorbing species could be a complex in which cysteine has added to the cofactor via its thiol group. Two possible structures are the simple thiohemiaminal complex and the cyclic thiazolidine in which both amine and thiol of cysteine have added to the cofactor. Arguments for *gem*-diamine as well as the proposed thiol·PLP interaction are presented in the Discussion section.

The apparent first-order rate constant for decay of this single intermediate to the stable complex varies hyperbolically with cysteine concentration, reaching a k_{max} of 220 s^{-1} and having a *y*-axis intercept of 33 s^{-1} and a K_d of 2.8 mM (Figure 2A). The simplest mechanism that can account for this dependence involves rapid formation of the 350 nm absorbing intermediate adduct followed by a single kinetically significant chemical step effecting conversion to the stable complex. In this scheme, k_{max} corresponds to the sum of the forward and reverse rate constants for the chemical step, the *y*-axis intercept corresponds to the reverse rate constant, and $K_{0.5}$ corresponds to the dissociation constant for formation of the 350 nm absorbing adduct. These relations would give $k_{forward} = 187 \pm 6$ s^{-1}, $k_{reverse} = 33 \pm 4$ s^{-1}, and $K_d = 2.8 \pm 0.3$ mM.

Substitution of the 2-position of the substrate with deuterium, which was shown above to be associated with a significant *equilibrium* isotope effect on the ratio of Cys aldimine to Cys ketimine species in the stable complex, results in, at most, a small (and inverse) *kinetic* isotope effect on the step associated with decay of the intermediate and formation of the stable complex. In monitoring the kinetics of this reaction, $k_{forward} = 214 \pm 8$ s^{-1}, $k_{reverse} = 44 \pm 5$ s^{-1}, and $K_d = 3.8 \pm 0.4$ mM were obtained (Figure 2A). Given the uncertainty that is typical for this sort of kinetic measurement, it is not clear that the differences between the values and their counterparts from the reaction with [2-^{1}H]cysteine are significant. The observation that there is a small inverse or insignificant kinetic effect on conversion of the intermediate into the stable complex but a comparatively large effect on the internal equilibrium associated with this state

requires that removal of the hydron from the 2-position not limit conversion of the intermediate to the stable complex. In other words, some step other than proton abstraction is rate-limiting for this conversion. This deduction would be consistent with the proposal that the initial adduct must rearrange to release the thiol of the substrate from the cofactor.

Kinetics of the Persulfide Formation Half-Reaction in CD0387. Stopped-flow analysis of the first half-reaction allowed resolution of six steps (Scheme 2). The first two are identical in character with those detected in the abortive reaction of the C326A variant protein. An intermediate with λ_{max} = 350 nm develops and gives way with apparent first-order rate constants of $k_{forward} = 90\ s^{-1}$ and $k_{reverse} = 13\ s^{-1}$ to a state with absorption maxima at ~340 and ~417 nm (Figure 4). This second state is subject to the same 2-^{2}H equilibrium isotope effect as the corresponding state in CD0387-C326A, as manifested by the change in the ratio of its two absorption features (Figure 2A). Thus, this state is proposed to comprise rapidly equilibrating Cys aldimine and Cys ketimine forms.

Step 3 in the reaction is the first step that is not observed in the CD0387-C326A reaction and, therefore, is most likely to correspond to the C−S bond-cleaving nucleophilic attack. Step 3 is defined by the development of long wavelength (~506 nm) absorption characteristic of a quinonoid form with retention of the 340 and 417 nm features of the ketimine and aldimine forms. The quinonoid species forms in a step subsequent to that in which the ketimine and aldimine are produced, as illustrated by the lag in development of A_{506} relative to A_{417} (Figure 5). This observation supports the notions that the 340/417 nm absorbing state comprises rapidly equilibrating Cys aldimine and Cys ketimine species whereas the 340/417/506 nm absorbing state comprises Ala aldimine, ketimine, and quinonoid forms. The rate constants for the step in which the quinonoid species accumulates given in Scheme 2 were obtained by iterative simulations of A_{506} versus time traces from reactions with different concentrations of cysteine (Figure 6).

As noted above, we propose that accumulation of the quinonoid species and C−S bond cleavage are associated with the same step. To probe the timing of C−S bond cleavage directly, a series of chemical-quench flow experiments was carried out. CD0387

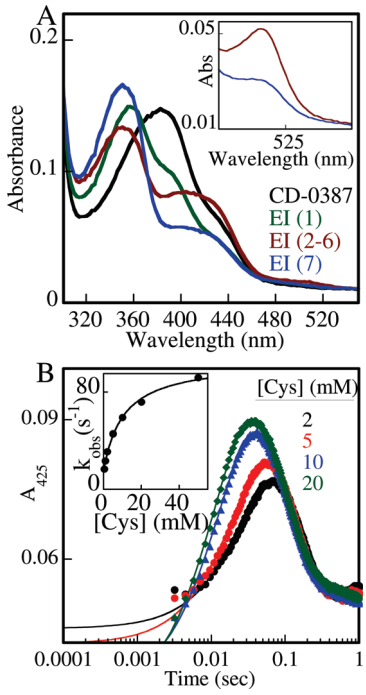

FIGURE 4: (A) Absorption spectra for the seven intermediates obtained from the data collected by multiwavelength stopped flow (Scheme 2). Thirty millimolar cysteine was added to 100 μM CD-0387 in 100 mM HEPES, pH 7.8 at 21 °C. The inset shows the low-energy absorption ascribed on the basis of literature precedent to a quinonoid form. (B) Kinetics of the development and decay of the 425 nm absorption after mixing cysteine with 100 μM CD-0387 (in 100 mM HEPES, pH 7.8) at 21 °C. The data are the fit of the equation for the double exponential, where the initial rise is dependent on cysteine concentration, while the second phase, a fall, is independent of cysteine concentration at 11−12 s^{-1}. The inset shows a plot of the rate constants obtained from the rise phase versus concentration of cysteine. The solid line is a fit of the equation for a hyperbola with a maximum of 90 s^{-1} and $k_{reverse}$ of 13 s^{-1}.

Scheme 2: Kinetic Mechanism Describing the First Half-Reaction ($EI_{(1)}$−$EI_{(6)}$) and the Inhibited Form of the Enzyme, $EI_{(7)}$

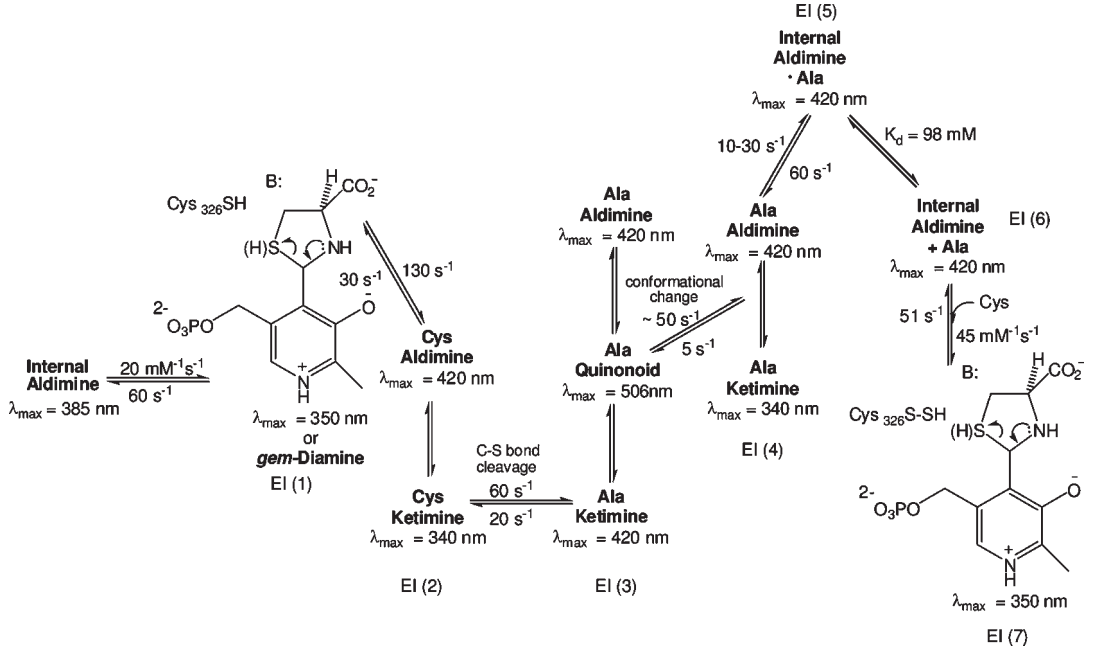

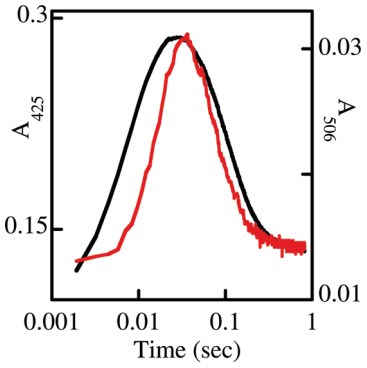

FIGURE 5: Comparison between the kinetic traces at 425 (black trace) and 506 (red trace) nm indicates that the 506 nm absorbing quinonoid species forms in a step distinct from that in which the ketimine and aldimine form and decay. Seventy millimolar cysteine was added to 50 μM CD0387.

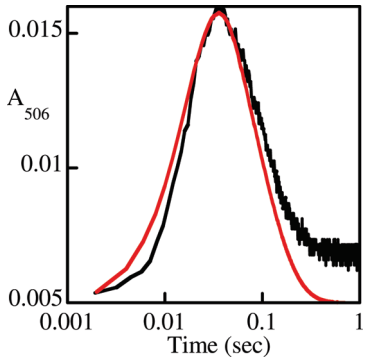

FIGURE 6: Kinetic simulation of the quinonoid species from the reaction of 20 mM cysteine with 100 μM CD0387. The black trace is the experimental kinetic trace, and the red line is the simulated kinetic trace.

was mixed with excess cysteine, the two were allowed to react for varying time, and the reaction mixture was then "quenched" by a mix with guanidine, base, and DTT (to cleave accumulated persulfide species). At higher concentrations of cysteine, the majority of the persulfide formation reaction was over within the earliest reaction time (5 ms). This could be taken as an indication that C−S bond cleavage occurs during formation of the first (350 nm absorbing) intermediate state, which occurs in the dead time of the stopped-flow apparatus for the majority of the enzyme. However, we favor the hypothesis that the enzyme is resistant to quenching and that, once the initial complex has formed, persulfide product is ultimately produced (or H_2S is produced directly by some alternative reaction) in spite of the subsequent mix with quench solution. Our rationale is twofold. First, similar results were obtained when 2 N H_2SO_4 was used as the quench solution, and, in this case, the bleaching of the PLP cofactor that occurs after denaturation was seen to occur slowly over seconds. This slow bleaching provides support for the notion that the enzyme resists rapid denaturation. Under single turnover conditions, reasonable kinetics and concentration dependencies were obtained, but due to limitations in accessible enzyme concentration, these experiments could not be used to distinguish the timing of C−S bond cleavage. Second, the reaction of the C326A variant protein exhibits the same first two steps as that of the wild-type protein, but no sulfur volatilization occurs in this case. Thus, we conclude that C−S bond cleavage correlates not with formation of the first intermediate state but with accumulation of the quinonoid species.

As Figure 5 illustrates, the 506 nm absorption characteristic of the putative Ala quinonoid species decays prior to decay of the 340 and 417 nm features associated with the Ala aldimine and Ala ketimine forms. As there is no obvious chemical step to be associated with decay of the quinonoid species, we propose that it reflects an enzyme conformational change that disfavors the quinonoid in its equilibrium with Ala aldimine and ketimine forms. Simulation of A_{417} and A_{506} versus time traces allowed rate constants of $k_{forward}$ of 50 s^{-1} and $k_{reverse}$ of 5 s^{-1} to be assigned to the conformational change. The intensity of the weak quinonoid-associated feature observed by mixing Ala with the preformed enzyme persulfide intermediate (*vide infra*) provided a crucial constraint for estimation of $k_{reverse}$.

The step associated with the lag in quinonoid development, in which the putative Cys aldimine/Cys ketimine state accumulates, exhibits at most a very small α-deuterium KIE, as revealed by comparison of the rise phases of A_{417} versus time traces for the reactions with deuterated and protiated cysteine (data not shown). Thus, the wild-type enzyme behaves similarly to the C326A variant protein in exhibiting a small or insignificant α-deuterium kinetic isotope effect on formation of the Cys aldimine/ketimine state. By contrast, A_{506} versus time traces from reactions of CD0387 with different concentrations of either [2-^{1}H]cysteine or [2-^{2}H]cysteine reveal that steps associated with quinonoid formation or decay (or both) are more sensitive to this isotopic substitution (Figure 7A). The most likely origin of the isotope effect on the kinetics of the quinonoid species is the aforementioned equilibrium effect on the Cys aldimine/Cys ketimine ratio. Because, according to the Dean and White mechanism (*1*), only the ketimine species can undergo C−S bond cleavage to allow for quinonoid accumulation, α-deuteration of the substrate, which favors Cys aldimine in its equilibrium with Cys ketimine, retards C−S bond cleavage. The A_{506} versus time traces can be accurately simulated by assuming a k_H/k_D of 1.8−2 only on the step in which the quinonoid species develops (Figure 7B). This effect accounts for both the slowing of A_{506} development and the reduction in amplitude associated with α deuteration. This k_H/k_D would correspond to a 1.8−2-fold reduction in the representation of the Cys ketimine form in its equilibrium with Cys aldimine. Conversely, reaction of CD0387 with [2-^{1}H]-L-cysteine in ^2H_2O, which is associated with a significant equilibrium isotope effect favoring Cys ketimine, should therefore give rise to an inverse solvent deuterium kinetic isotope effect on the rate constant for C−S bond cleavage and development of the quinonoid form. In this case, analysis of the kinetic data to evaluate this prediction is complicated by the fact that the steps surrounding the step in question are all subject to significant *normal* solvent KIEs. The step preceding quinonoid development, characterized by an increase in A_{417}, exhibits the largest effect of between 2 and 3 (Figure 8A). A similar effect is seen in this step in the reaction of CD0387-C326A (data not shown). Thus, the lag phase in quinonoid development should be longer in ^2H_2O, an expectation that is borne out by the comparison shown in Figure 8B. The step in which the quinonoid species decays, which is proposed to be a protein conformational change, exhibits a somewhat smaller normal effect of approximately 1.8 (Figure 8C). The last step, in which the absorption of the aldimine decays and that of the inhibited complex develops, also exhibits a normal effect of nearly 2 (Figure 8A). The challenge, then, is to discern whether the overall slowing of quinonoid development and decay caused by the sizable normal

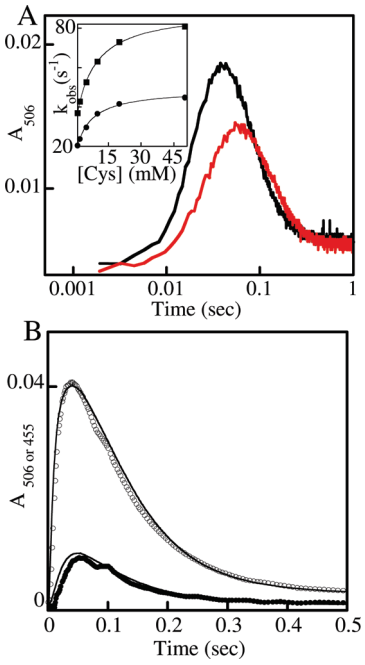

FIGURE 7: (A) The kinetics of both the formation and decay of the 506 nm absorbing feature (Ala quinonoid) are affected by a factor of 2.2−2.5 by α deuteration. Ten millimolar [2-^{2}H]cysteine (red trace) or [2-^{1}H]cysteine (black trace) was added to 100 μM C326A in 100 mM HEPES, pH 7.8 at 21 °C. The inset shows the rate constants obtained from the fits on the rise phase versus cysteine concentration. The solid lines in the inset are the fit of the equation for a hyperbola (squares for protiated cysteine and circles for deuterated cysteine). (B) Kinetic simulations of formation and decay of the aldimine (open circles) and quinonoid (closed circles) species from the reaction of 20 mM L-cysteine with 100 μM CD0387 (in 100 mM HEPES, pH 7.8 at 21 °C). The solid lines are the simulated kinetic traces.

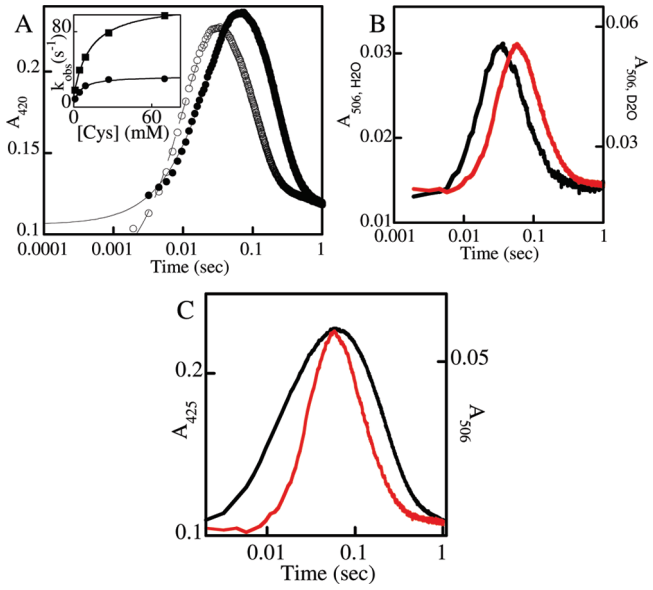

FIGURE 8: (A) Solvent deuterium kinetic isotope effect of 2−3 on the formation and decay of the 425 nm absorbing feature. Open circle kinetic traces are in H_2O, and filled circle kinetic traces are in ^2H_2O. The inset shows a plot of the rate constants obtained from the rise phase versus concentration of cysteine. The solid lines in the inset are the fit of the equation for a hyperbola (squares for protonated solvent and circles for deuterated solvent). (B) Solvent kinetic isotope effect on the formation of the putative Ala quinonoid. The plot shows absorbance traces at 506 nm in ^2H_2O (red trace) versus H_2O (black trace) solvents. Seventy millimolar cysteine was added to 100 μM CD-0387 (in 100 mM HEPES, pH 7.8) at 21 °C. (C) Comparison between the kinetic traces at 425 and 506 nm in ^2H_2O indicates that the 506 nm trace (red) maximizes earlier than the 425 nm trace (black). Stopped-flow data were obtained after mixing 70 mM Cys with 50 μM CD-0387 in 100 mM HEPES, pD 7.8 at room temperature. t_{max} = 58 and 63 ms for the 506 and 425 species, respectively.

solvent KIEs on the steps surrounding that in which the species actually forms masks an inverse effect on the formation step. Comparison of absorbance versus time traces at selected wavelengths and kinetic simulations indicate that this is the case. Superposition of the A_{417} and A_{506} versus time traces for the reaction with high cysteine concentrations in H_2O shows that the time of maximum absorbance is significantly greater for the latter than for the former (Figure 5). This observation is readily reproduced by a simulation employing the rate constants shown in Table 1. By contrast, the same comparison for the reaction in ^2H_2O shows that the time of maximum absorbance at 506 nm is actually less than that at 417 nm (Figure 8C). With appropriate normal solvent isotope effects for the three steps surrounding that in which the quinonoid species forms (2.3 for the step in which the Cys aldimine/ketimine state develops and 1.8 for the steps in which the Ala aldimine/quinonoid/ketimine and Ala aldimine/ketimine states decay) and the assumption of equivalent solvent ^{2}H-KIEs on forward and reverse reactions (i.e., no net solvent ^{2}H-EIEs on these individual steps), the shifts in t_{max} values could be reproduced by simulations invoking an inverse effect of $k(^1H_2O)/k(^2H_2O)$ = 0.67−0.83 on the step in which the aldimine/quinonoid/ketimine state forms. These simulations also correctly predict an increase in the amplitude of the transient 506 nm absorption, although they do not account for the entire increase that is observed. The demonstrated equilibrium solvent isotope effect on aldimine/ketimine ratio must also tend to favor the quinonoid species in the internal equilibrium associated with the Ala aldmine/quinonoid/ketimine state. The important point is that the data are consistent with an inverse solvent ^{2}H-KIE originating from a ketimine-favoring solvent ^{2}H-EIE effect on the putative Cys aldimine/ketimine state. This observation validates the assignment of the intermediate state.

The remaining three steps in Scheme 2 appear as a single step in stopped-flow monitoring of the reaction of CD0387 with excess cysteine. This single observed step is defined by loss of the 340 and 417 nm absorptions of the putative Ala aldimine/ketimine state and development of a new absorption feature at 345 nm with an apparent first-order rate constant of 12 s^{-1}. The final, stable complex arises from combination of the enzyme's persulfide form (produced upon reaction of the first molecule of cysteine) with a second molecule of the substrate. With the position of its absorption feature, this complex must lack conjugation between the pyridoxal ring and the iminium moiety. This loss of conjugation arises either from thiol addition to the iminium of the internal aldimine or from progression to a persulfide/Cys ketimine form of the enzyme, which is expected to accumulate due to the incompetency of the persulfide enzyme for the subsequent C−S bond-cleaving nucleophilic attack.

This last observed step is subject to a significant normal α-^{2}H-KIE of 1.4 ± 0.1 at all concentrations of cysteine (Figure 9). The A_{417} versus time traces can be simulated by assuming that the ^{2}H-KIE observed in the fall phase actually arises from the step in which the quinonoid species develops. In other words, because rate constants for the steps are similar, the retardation of the C−S bond cleavage step that results from the equilibrium effect on the Cys aldimine/ketimine state is propagated into the kinetic phase

Table 1: Kinetic Parameters Used in Simulations Designed To Resolve the Solvent Isotope Effect in the Reaction of Cysteine with CD0387[a]

	binding		425 nm		506 nm		conformational change		product release	
solvent	k_{on} ($M^{-1}s^{-1}$)	k_{off}	k_{for}	k_{rev}	k_{for}	k_{rev}	k_{for}	k_{rev}	k_{for}	k_{rev}
H_2O	2×10^5	700	130	30	60	20	40	5	30	0
D_2O	5×10^4	300	48	13	60	20	20	2.5	15	0

[a]The unit for all rate constants except the "binding step" is s^{-1}.

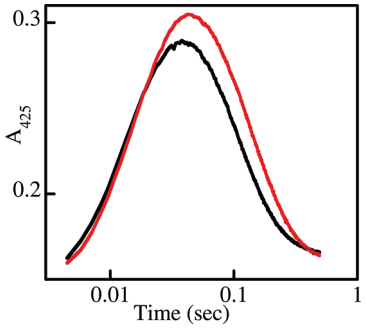

FIGURE 9: Kinetic isotope effect of 1.4 observed on the decay of the 425 nm-absorbing feature. Kinetic traces show the development and decay of the 425 nm absorbing feature after mixing 10 mM [2-^{2}H]cysteine (red trace) or [2-^{1}H]cysteine (black trace) with 100 μM CD-0387 (in 100 mM HEPES, pH 7.8) at 21 °C.

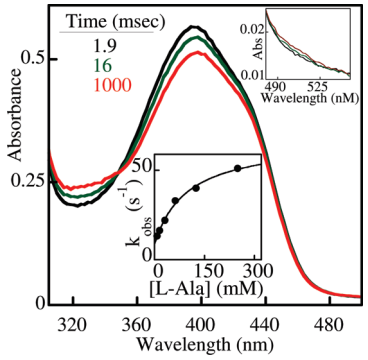

FIGURE 10: Binding of Ala to the persulfide exhibits saturation kinetics. Spectra show changes in the absorption spectrum of the persulfide upon addition of Ala at various time points. The top inset shows the formation of the putative Ala quinonoid, and the center inset depicts the rate constants acquired from the global analysis for formation of the putative Ala ketimine versus Ala concentration. The data are the fit of the equation for a hyperbola with $k_{max} = 60\ s^{-1}$, $k_{off} = 10\ s^{-1}$, and $K_d = 98$ mM.

associated with the subsequent steps leading to the formation of the 345 nm absorbing persulfide·Cys adduct.

The kinetics of the individual steps that constitute the transition from the Ala aldimine/ketimine state to the persulfide·Cys complex could be resolved by stopped-flow experiments in which the persulfide form of the enzyme, which was prepared by a prior incubation of resting CD0387 with stoichiometric substrate, was mixed with either cysteine or alanine. In the former reaction, complex formation was shown by variation of [Cys] to exhibit second-order kinetics with rate constants of $k_{forward} = 45\ mM^{-1}\ s^{-1}$ and $k_{reverse} = 51\ s^{-1}$ (data not shown). These rate constants lead to a calculated dissociation constant of 1.2 mM. Direct titration of the enzyme with excess cysteine (data not shown) gave a similar K_d. The formation of this adduct can explain the substrate inhibition observed with CD-0387 and CD-0704 (*13*, *15*) if it is assumed that binding of the second cysteine inhibits persulfide cleavage. We previously concluded that persulfide cleavage by dithiols such as DTT is initiated by prior formation of an adduct between the cofactor and one of the two thiols (*13*). In view of this mechanism, occupation of the cofactor site by cysteine is, in fact, anticipated to inhibit persulfide cleavage, leading to the observed substrate inhibition in the steady state.

The steps in which alanine is released from the cofactor and then dissociates from the persulfide form of the enzyme were resolved by mixing the persulfide with alanine. This reaction leads to spectral changes in the 340 and 417 nm region (Figure 10), presumably as a result of formation of the external (Ala) aldimine and, after rapid proton transfers, Ala ketimine. In addition, as predicted by kinetic Scheme 2, Ala quinonoid accumulates (inset to Figure 10). The small amplitude of the 506 nm feature as the quinonoid is formed in the reverse direction compared to that for its formation in the forward direction is consistent with a forward-favoring equilibrium constant for the enzyme conformational change. Formation of the putative Ala aldimine/quinonoid/ketimine state shows no lag phase, and the observed first-order rate constant for formation saturates with a k_{max} of $70\ s^{-1}$, a y-axis intercept of $10\ s^{-1}$, and a $K_{0.5}$ of 98 mM (inset to Figure 10). Thus, the simplest mechanism that can account for the kinetic data includes rapid-equilibrium binding of Ala and a subsequent chemical step in which the external aldimine is converted into the Ala aldimine/quinonoid/ketimine state. In this mechanism, $K_{0.5}$ reflects K_d for Ala binding (noncovalently) to the enzyme in the rapid-equilibrium step, k_{max} reflects the sum of k_{on} and k_{off} for alanine adding to the cofactor, and the y-axis intercept reflects k_{off}. The value of $10\ s^{-1}$ for the latter is in reasonable agreement with the rate constant deduced for this step from analysis of the stopped-flow data on the forward reaction. This rate constant agrees well with the previously reported value of k_{cat} for turnover in the presence of tris(2-carboxyethyl)phosphine, a persulfide cleaver efficient enough to render the persulfide-formation half-reaction completely rate-limiting (*13*). Thus, the previous and present study identify release of product alanine from the cofactor as the rate-limiting step in the presence of an optimized acceptor for the persulfide sulfur.

The amplitude of the change at 340 nm, which reflects the population of the ketimine at equilibrium, is decreased when the persulfide enzyme is reacted with [2-^{2}H]-L-alanine (data not shown). Conversely, the ketimine absorption develops to a greater extent when the persulfide is mixed with [2-^{1}H]-L-alanine in ^2H_2O. Thus, the equilibrium isotope effects observed for cysteine in the forward direction are also observed for Ala in the reverse direction.

DISCUSSION

The spectral/kinetic data obtained for the reactions of CD0387 and its C326A variant with [2-^{1}H]cysteine and [2-^{2}H]cysteine can largely be accommodated within the context of the chemical

mechanism first proposed by White, Dean, and co-workers (Scheme 1). The identity of the first intermediate is most notable. A *gem*-diamine adduct, which has been observed with numerous PLP-dependent enzymes, is a reasonable assignment for the 350 nm-absorbing species (*16*, *17*). species. The initial combination of cysteine via its thiol is another possibility. This step would seem to be counterproductive, as addition of the thiol does not establish the necessary conjugation to facilitate α-proton abstraction. (Indeed, in the proposed thiazolidine structure, thiol addition would even appear to antagonize the desired proton abstraction.) The evidence for this proposal is indirect and warrants summary. First and foremost, thiol compounds such as DTT and 2-mercaptoethanol can add to the cofactor and form complexes with absorption spectra that are virtually identical with that of the intermediate (*18*). All small thiol compounds that we tested were able to effect the spectral change, albeit with markedly different concentration dependencies, whereas no non-thiol compound gave the same spectral change. Second, these thiol compounds and cysteine all react with the wild-type enzyme with at least one kinetic phase that is demonstrably first order in ligand. By contrast, addition of alanine to the persulfide form of CD0387 shows clear evidence for a binding step preceding the step in which the product combines with the cofactor, and the complex that subsequently forms has a very different absorption spectrum. This complex becomes predominant only at concentrations of alanine that are very high compared to the concentrations of thiol compounds (which are not natural substrates for the enzyme) required to drive complex formation. Third, the kinetics of the initial binding of cysteine to the free enzyme and binding to form the persulfide·Cys complex (the inhibited form) are essentially the same.

The assignment of the first intermediate as a thiol-adducted enzyme·cysteine complex raises the issue of the functional importance of this complex. One possibility is that it forms simply as a consequence of the greater inherent nucleophilicity of the thiol functional group in comparison with the amine and has no functional importance. We consider it more likely that formation of the adduct reflects an important design principle of the desulfurase active site. First, the enzyme may exploit the thiol−cofactor interaction to engender specificity for its substrate with respect to other (non-thiol) amino acids. This strategy of capturing the substrate's amine group by prior interaction with its thiol would seem roughly analogous to that used in protein ligation technology, in which formation of an amide is mediated by prior thioester formation via the thiol of the N-terminal cysteine in the attacking peptide. Second, the enzyme may, for some other purpose, bind cysteine in a conformation in which the thiol is directed toward the electrophilic C-4′ of the cofactor. What might that purpose be? One mechanistic imperative for successful desulfurase function is avoidance of the elimination of sulfide from the cysteine·PLP adduct, a reaction that is mediated by other PLP-dependent enzymes (cyst(e)ine C−S lyase). Our characterization of CD0387-C326A indicates that its active site accomplishes this imperative exquisitely. One possible strategy for suppression of this alternative reactivity is reduction of the lifetime of the quinonoid intermediate, which would drive the 1,2-elimination via its resonance-stabilized, C2-centered carbanion. This could be accomplished by ensuring rapid protonation of the C4′ of the cofactor following abstraction of the substrate α-proton. The thiol group of cysteine could, if directed at this carbon, mediate the rapid protonation step. Our interpretation that the quinonoid species accumulates only after cleavage of the thiol from the amino acid is consistent with this notion. Thus, the putative thiol may add to the cofactor as a consequence of the enzyme's strategy of directing it toward the cofactor to serve as general acid.

The significant ^{2}H-EIEs (solvent and substrate/product α-^{2}H) on the ratio of the putative rapidly interconverting aldimine/(quinonoid)/ketimine states have several important implications for the kinetics and mechanism of CD0387. First, the persistence of this effect for many seconds even with small excesses of substrate suggests that the exchange is slow compared to even the slowest steps in the persulfide formation sequence. This conclusion would be at odds with that reached for *A. vinelandii* NifS. On the basis of the complete exchange of the α-hydrogen in unreacted cysteine, it was concluded that substrate addition to the cofactor and α-proton abstraction and exchange are all fast compared with the C−S bond cleavage step. It is very possible, however, that the exchange observed by Dean and co-workers did not occur during the first half-turnover (conversion of the resting enzyme to the persulfide species) but instead was catalyzed by the persulfide form of the enzyme, which would have accumulated to stoichiometry under the conditions employed (in the absence of a reducing cosubstrate). Thus, the observed exchange might not be relevant to the first half-turnover.

A second implication of the observed 2-^{2}H equilibrium isotope effect is that the conjugate acid of the α-proton abstracting base is almost certainly monoprotic, providing argument against the lysine of the internal aldimine, a residue that has been proposed as the abstracting base in other PLP-dependent enzymes, as a candidate. The basis for this argument is that the presence of three protons on the conjugate acid of the α-proton-abstracting base would reduce the magnitude of the observed equilibrium isotope effect, such that even a very large intrinsic effect of 2 could give rise to an observed effect of only 1.33. The actual observed effect is probably greater than 1.33. The certainty of this conclusion is tempered by the difficulty in accurately determining the magnitude of the effect, which relates to the general convolution of species concentrations and molar absorptivities in analysis of absorption data. However, the notion that the α-proton-abstracting base is not lysine is bolstered somewhat by the knowledge that amines generally have fractionation factors greater than unity, which in this instance should give rise to a substrate ^{2}H-EIE favoring ketimine rather than aldimine.

It can be stated with greater confidence that the net 1,3-prototropic shift that interconverts the aldimine and ketimine species is mediated by a pair of acidic/basic residues rather than a single base and its conjugate acid. The fractionation factors for the α-proton in the aldimine species and the C-4′ proton in the ketimine species are expected to be very similar. Thus, only a very small substrate ^{2}H-EIE would be expected were a single residue to mediate the rapid 1,3-transfer. Moreover, the opposing effects of solvent and substrate deuterium on the equilibrium provide additional evidence that a two-base mechanism is operant.

Although it is impossible to quantify the ^{2}H-EIEs, they are clearly sufficiently large to suggest the participation of basic/acidic residues with unusual fractionation factors. One seemingly attractive possibility is that a cysteine residue is responsible for abstraction of the α-proton. In this scenario, the very small fractionation factor of the thiol could give rise to a ^{2}H-EIE in excess of 2 in favor of aldimine. However, the nucleophilic cysteine cannot be the α-proton-abstracting base, because the C326A variant protein exhibits no apparent defect in proton abstraction. Furthermore, the published structures of other cysteine desulfurases do not show another cysteine in an appropriate

position in the active site. Thus, the identity of the base and the mechanism by which the large equilibrium effect is engendered remain unclear. Conversely, the large solvent ^{2}H-EIE in favor of ketimine would be accommodated well by the proposed delivery of the proton to C-4′ of the cofactor by the thiol of the substrate itself.

Our kinetic dissection of the persulfide-forming half-reaction of a CD reveals that, as with many other enzyme reactions, no one single step is exclusively rate-limiting. Interestingly, the C−S-cleaving nucleophilic attack step, which is unique to this family of enzymes and has been proposed to be rate-limiting, is not even the slowest step. This raises the question of how the enzyme poises the ketimine adduct to promote the attack. The kinetic characterization of the wild-type enzyme sets the stage for detailed characterization of variant proteins to elucidate the function of specific residues in promoting steps in the reaction.

REFERENCES

1. Zheng, L., White, R. H., Cash, V. L., and Dean, D. R. (1994) Mechanism for the desulfurization of L-cysteine catalyzed by the nifS gene product. *Biochemistry 33*, 4714–4720.
2. Zheng, L., White, R. H., Cash, V. L., Jack, R. F., and Dean, D. R. (1993) Cysteine desulfurase activity indicates a role for NIFS in metallocluster biosynthesis. *Proc. Natl. Acad. Sci. U.S.A. 90*, 2754–2758.
3. Zheng, L., and Dean, D. R. (1994) Catalytic formation of a nitrogenase iron-sulfur cluster. *J. Biol. Chem. 269*, 18723–18726.
4. Yuvaniyama, P., Agar, J. N., Cash, V. L., Johnson, M. K., and Dean, D. R. (2000) NifS-directed assembly of a transient [2Fe-2S] cluster within the NifU protein. *Proc. Natl. Acad. Sci. U.S.A 97*, 599–604.
5. Kessler, D. (2006) Enzymatic activation of sulfur for incorporation into biomolecules in prokaryotes. *FEMS Microbiol. Rev. 30*, 825–840.
6. Jacobson, M. R., Cash, V. L., Weiss, M. C., Laird, N. F., Newton, W. E., and Dean, D. R. (1989) Biochemical and genetic analysis of the nifUSVWZM cluster from *Azotobacter vinelandii*. *Mol. Gen. Genet. 219*, 49–57.
7. Nakai, Y., Yoshihara, Y., Hayashi, H., and Kagamiyama, H. (1998) cDNA cloning and characterization of nouse nifS-like protein, m-Nfs1: mitochondrial localization of eukaryotic NifS-like proteins. *FEBS Lett. 433*, 143–148.
8. Kispal, G., Csere, P., Prohl, C., and Lill, R. (1999) The mitochondrial proteins Atm1p and Nfs1p are essential for biogenesis of cytosolic Fe/S proteins. *EMBO J. 18*, 3981–3989.
9. Smith, A. D., Agar, J. N., Johnson, K. A., Frazzon, J., Amster, I. J., Dean, D. R., and Johnson, M. K. (2001) Sulfur transfer from IscS to IscU: the first step in iron-sulfur cluster biosynthesis. *J. Am. Chem. Soc. 123*, 11103–11104.
10. Urbina, H. D., Silberg, J. J., Hoff, K. G., and Vickery, L. E. (2001) Transfer of sulfur from IscS to IscU during Fe/S cluster assembly. *J. Biol. Chem. 276*, 44521–44526.
11. Krebs, C., Agar, J. N., Smith, A. D., Frazzon, J., Dean, D. R., Huynh, B. H., and Johnson, M. K. (2001) IscA, an alternate scaffold for Fe-S cluster biosynthesis. *Biochemistry 40*, 14069–14080.
12. Kato, S., Mihara, H., Kurihara, T., Takahashi, Y., Tokumoto, U., Yoshimura, T., and Esaki, N. (2002) Cys-328 of IscS and Cys-63 of IscU are the sites of disulfide bridge formation in a covalently bound IscS/IscU complex: implications for the mechanism of iron-sulfur cluster assembly. *Proc. Natl. Acad. Sci. U.S.A. 99*, 5948–5952.
13. Behshad, E., Parkin, S. A., and Bollinger, J. M. (2004) Mechanism of cysteine desulfurase Slr0387 from *Synechocystis* sp. PCC 6803: kinetic analysis of cleavage of the persulfide intermediate by chemical reductants. *Biochemistry 43*, 12220–12226.
14. Han, J. C., and Han, G. Y. (1994) A procedure for quantitative determination of tris(2-carboxyethyl)phosphine, an odorless reducing agent more stable and effective than dithiothreitol. *Anal. Biochem. 220*, 5–10.
15. Parkin, S. A. (1998) Physiological and mechanistic studies of cysteine desulfurases from *Synechocystis* sp. PCC 6803, Masters Thesis, The Pennsylvania State University, University Park, PA.
16. Phillips, R. S., Bender, S. L., Brzovic, P., and Dunn, M. F. (1990) The mechanism of binding of substrate analogues to tryptophan indole-lyase: studies using rapid-scanning and single wavelength stopped-flow spectrophotometry. *Biochemistry 29*, 8608–8614.
17. Karsten, W. E., and Cook, P. F. (2009) Detection of a *gem*-diamine and a stable quinonoid intermediate in the reaction catalyzed by serine−glyoxylate aminotransferase from *Hyphomicrobium methylovorum*. *Biochim. Biophys. Acta 6*, 575–580.
18. Buell, M. V., and Hanse, R. E. (1960) Reaction of pyridoxal phosphate with aminothiols. *J. Am. Chem. Soc. 82*, 6042–6049.